

Numerical Investigation of the Turbulent Wake of Generic Space Launchers

S. Loosen, V. Statnikov, M. Meinke, and W. Schröder

Abstract The turbulent wakes of generic space launchers are numerically investigated via a zonal RANS/LES method and optimized dynamic mode decomposition (DMD), to gain insight into characteristic wake flow modes being responsible for asymmetrical loads on the engine extension known as buffet loads. The considered launcher geometries range from planar space launchers up to axisymmetric free flight configurations investigated at varying free stream conditions, i.e. transonic and supersonic. The investigated wake topologies reveal a highly unsteady behavior of the shear layer and the separation region resulting in strongly periodic and antisymmetric wall pressure fluctuations on the nozzle surface. Using conventional spectral analysis and dynamic mode decomposition, several spatio-temporal coherent low frequency modes which are responsible for the detected pressure oscillations are identified. In addition, a passive flow control device consisting of semi-circular lobes integrated at the base shoulder of the planar configuration is investigated. The objective of the concept is to reduce the reattachment length and thus the lever arm of the forces as well as to stabilize the separated shear layer. The results show a significant reduction of the reattachment length by about 75%. In addition, the semi-circular lobes partially reduce undesired low frequency pressure fluctuations on the nozzle surface. However, this reduction is achieved at the expense of an increase of high frequency pressure fluctuations due to intensified small turbulent scales.

1 Introduction

The tail of a classical space launcher, e.g., ARIANE 5, TITAN 4, H-II to name a few, includes an abrupt junction between the main body and the attached rocket engine causing the boundary layer to separate on the base shoulder. According to the varying freestream (sub-, trans-, supersonic) and nozzle flow conditions (over-expanded, adapted, underexpanded), the shed turbulent shear layer subsequently reattaches on the nozzle wall or intensively interacts with the emanating jet plume.

S. Loosen (✉) • V. Statnikov • M. Meinke • W. Schröder
Institute of Aerodynamics, RWTH Aachen University, Wüllnerstraße 5a, 52062 Aachen,
Germany
e-mail: s.loosen@aia.rwth-aachen.de

For an ARIANE 5-like launcher, aerodynamically most critical is the early transonic part of the flight trajectory. At this stage, the turbulent shear layer shed from the main body impinges on the nozzle just upstream of its end, which due to high dynamic pressure values leads to significant wall pressure fluctuations. The resulting unsteady aerodynamic forces known as the buffet phenomenon, can lead under unfavorable conditions to a complete loss of the vehicle. Unfortunately, unlike the rocket inner engine flow the wake flow of a real launcher cannot be analyzed in full-scale on the ground, leading to increased safety margins and consequently, a reduced launcher efficiency. Therefore, accurate numerical tools validated by high-fidelity experimental investigations are required to provide detailed insight into the wake flow phenomena, to develop methods of their controllability, and to ultimately reduce aerodynamic loads on the nozzle structure without penalizing the launcher's efficiency.

The turbulent wake flow exhibits many similarities with the separated shear flow behind a backward-facing step (BFS). The flow over a BFS has been extensively studied experimentally, e.g., by Bradshaw and Wong [2], Eaton and Johnston [6], Simpson [24], and Driver et al. [5], and numerically, e.g., by Le et al. [14], Silveira Neto et al. [23], Friedrich and Arnal [8], and Kaltenbach and Janke [12]. In all the investigations a variation of the instantaneous impingement location of the separated shear layer by about two step heights around the mean reattachment position is reported. In addition, two basic modes of characteristic frequencies were detected in nearly all of the above mentioned studies. The low frequency mode at a Strouhal number of $Sr_h = 0.012\text{--}0.014$ based on the step height and the free stream velocity reflects an overall enlarging and contraction of the separation bubble or shear-layer "flapping" as it is commonly called in the literature. The aforementioned time dependent variation of the instantaneous reattachment position can be attributed to this "flapping" motion. Besides the investigations on planar configurations a lot of research has been done on axisymmetric space launchers at transonic speed [3, 4, 15, 21]. Schrijer et al. [21] detected by proper orthogonal decomposition (POD) two dominant wake modes containing the majority of the turbulent kinetic energy. The first low frequency mode captures a oscillating growing and shrinking of the separation zone most probably being the counterpart of the shear-layer "flapping" detected in the planar BFS flows. The second higher frequency mode describes an undulating motion of the shear layer, thus, coinciding with the vortex-shedding of the BFS flow [14]. Deprés et al. [4] and Deck and Thorigny [3] performed a two-point correlation analysis in the wake of an axisymmetric configuration and detected an anti-phase oscillation with $Sr_D \approx 0.2$ in the instantaneous wall pressure signal located at opposite sides in the azimuthal direction.

For the development of efficient lightweight space launchers it is essential to decrease the low frequency dynamic loads arising due to such large scale coherent motions. One promising possibility to manipulate the flow field and to reduce these loads is passive flow control. First applications of passive flow control in conjunction with space launchers can be traced back to the second half of the last century. Modified main bodies such as boat tails were extensively investigated [22] to increase the base pressure and thereby to reduce the overall drag. However,

the purpose of the majority of the control devices examined in the recent past is a reduction of the reattachment length and thus the momentum arm to decrease the dynamic bending moments. It has been demonstrated that streamwise vortices intensify the turbulent mixing in the shear layer just downstream of the BFS leading to an increasing entrainment and spreading of the shear layer and consequently to a reduced reattachment length [10, 16]. Using tabs [16], chevrons [20], and castellation-like geometries [9] the reattachment length was reduced by up to 50%. The most promising approach to decrease the reattachment length is the so-called lobed mixer initially developed to reduce the noise in jet engines [31] but more recently also applied to a BFS configuration [1]. Due to the interaction of the spanwise and streamwise vortices generated by the lobes, the flow behind the lobed mixer becomes fully three-dimensional leading to an accelerated reattachment [24].

Within the project the turbulent wake of various ARIANE 5-like configuration is investigated at transonic and supersonic freestream conditions using a zonal RANS/LES approach and Dynamic Mode Decomposition, to detect characteristic wake flow modes responsible for the buffeting phenomenon. A large number of various configurations including planar space launchers as well as axisymmetric free flight configurations are investigated. In addition, the effect of a passive flow control device, consisting of semi-circular lobes integrated at the base shoulder, on the wake of a generic planar model is investigated.

1.1 Zonal RANS/LES Flow Solver

The time-resolved numerical computations are performed using a zonal RANS-LES finite-volume method. The computational domain is split into different zones. In the zones where the flow is attached, which applies to the flow around the forebody and insight the nozzle, the RANS equations are solved. The wake flow characterized by the separation and a pronounced dynamic is determined by an LES. The Navier-Stokes equations of a three-dimensional unsteady compressible fluid are discretized second-order accurate by a mixed centered/upwind advective upstream splitting method (AUSM) scheme for the Euler terms. The non-Euler terms are approximated second-order accurate using a centered scheme. For the temporal integration an explicit 5-stage Runge-Kutta method of second-order accuracy is used. The monotone integrated LES (MILES) method determines the impact of the sub-grid scales. The solution of the RANS equations is based on the same discretization schemes. To close the time-averaged equations the one-equation turbulence model of Fares and Schröder [7] is used. For a comprehensive description of the flow solver see Statnikov et al. [26, 27].

The transition from the RANS to the LES domain is determined by the reformulated synthetic turbulence generation (RSTG) method developed by Roidl et al. [17, 18]. Using this method, a reconstruction of the time-resolved turbulent fluctuations in the LES inlet plane by the upstream RANS solution is realized. Following the synthetic eddy method (SEM) by Jarrin et al. [11], turbulence is

described as a superposition of coherent structures. The structures are generated at the inlet plane by superimposed virtual eddy cores. These eddy cores are defined at random positions \mathbf{x}_i in a virtual volume V_{virt} which encloses the inlet plane and exhibits the dimension of the turbulent length scale l_x , the boundary-layer thickness at the inlet δ_0 , and the width of the computational domain L_z in the streamwise, the wall-normal, and the spanwise direction. To take the inhomogeneity of the turbulent scales in the wall-normal direction into account, the virtual eddy cores are described by different shape factors and length and time scales depending on the wall-normal distance. Having N synthetic eddies, the normalized stochastic velocity fluctuations u'_m at the LES inlet plane are determined by the sum of the contribution $u_m^i(\mathbf{x}, t)$ of each eddy core i

$$u'_m(\mathbf{x}, t) = \frac{1}{\sqrt{N}} \sum_{i=1}^N \underbrace{\epsilon_i f_{\sigma,m}^i(\mathbf{x} - \mathbf{x}_i)}_{u_m^i(\mathbf{x}, t)} \quad (1)$$

with ϵ_i being a random number within the interval $[-1, 1]$, $f_{\sigma,m}^i$ being the shape function of the respective eddy, and $m = 1, 2, 3$ denoting the Cartesian coordinates in the streamwise, the wall-normal, and the spanwise direction. The final velocity components at the LES inflow plane u_m are composed of an averaged velocity component $u_{RANS,m}$ from the RANS solution and the normalized velocity fluctuations u'_m which are subjected to a Cholesky decomposition A_{mn} to assign the values of the target Reynolds-stress tensor $R_{mn} = A_{mn}^T A_{mn}$ corresponding to the turbulent eddy viscosity of the upstream RANS

$$u_m(\mathbf{x}, t) = u_{RANS,m} + A_{mn} u'_m(\mathbf{x}, t). \quad (2)$$

To enable an upstream information exchange, thus, a full bidirectional coupling of the two zones, the static pressure of the LES zone is imposed after a transition of three boundary-layer thicknesses at the end of the overlapping zone onto the RANS outflow boundary. The temporal window width used to compute the pressure for the RANS outflow plane is chosen such that high-frequency oscillation of the LES pressure field are filtered out. A more detailed description of the zonal RANS/LES method specifying the shape functions and length scales is given in [17, 18].

2 Results

Within this section the results of the simulations performed within the last funding period are presented. The chapter is divided into three parts, each dealing with a different space launcher geometry and free stream conditions.

2.1 Transonic Planar Backward-Facing Step Configuration

To illustrate the flow topology along the investigated generic space launcher configuration, the instantaneous Mach number and wall pressure coefficient distributions are presented in Fig. 1a. The incoming freestream with $Ma_\infty = 0.8$ and $Re_{D^*} = 6 \cdot 10^5$ passes over the transonic nose of the model, locally accelerating to $Ma \approx 0.9$ and subsequently decelerating to $Ma_\infty \approx 0.8$ near the end of the forebody. At the abrupt backward-facing step at the end of the forebody, the turbulent boundary layer separates and forms a turbulent shear layer. The shed shear layer rapidly develops downstream of the separation due to the shear layer instability, causing the mixing layer and thus the turbulent structures to grow in size and intensity. Further downstream, the shear layer gradually approximates the lower wall and finally impinges on it over a relatively wide distance in the streamwise direction between $4 \lesssim x_r/h \lesssim 9$ depending on the time instance and the spanwise position. Moreover, as can be seen in the instantaneous skin-friction coefficient distributions shown in Fig. 1b, despite the quasi-2D geometry of the step there are rather wedge-shaped reattachment spots than a straight reattachment line which strongly oscillate in the streamwise and the spanwise directions.

To provide insight into temporal periodicity aspects of the wake flow dynamics and the resulting structural loads, the power spectral density (PSD) is computed of the wall pressure signals at selected positions within the shear layer reattachment region. The resulting PSD spectra are shown in Fig. 2a. At $x = 1.5D$, one distinct peak can be clearly identified at $Sr_{D^*} \approx 0.04$. The spectrum at the

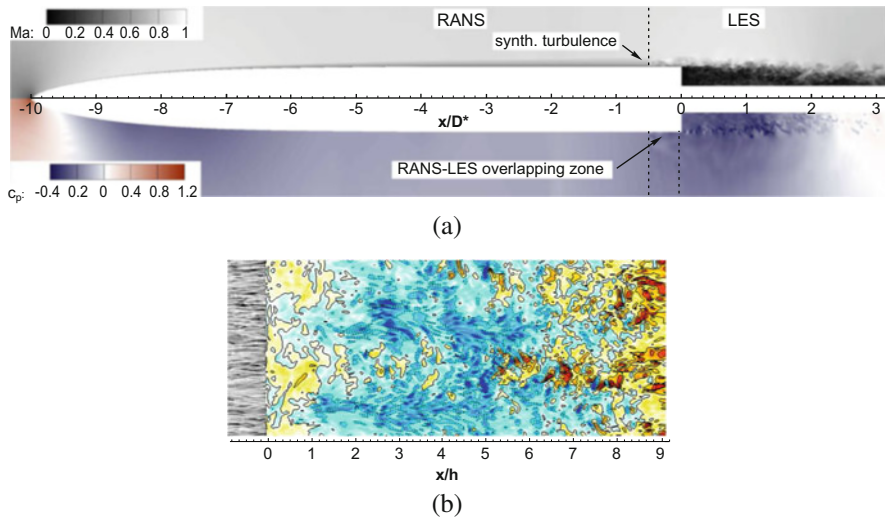


Fig. 1 (a) Flow topology of the investigated generic space launcher configuration [27]: Instantaneous Mach number (upper half) and pressure coefficient (lower half) distributions. (b) Skin-friction coefficient distribution on the main body and the splitter plate

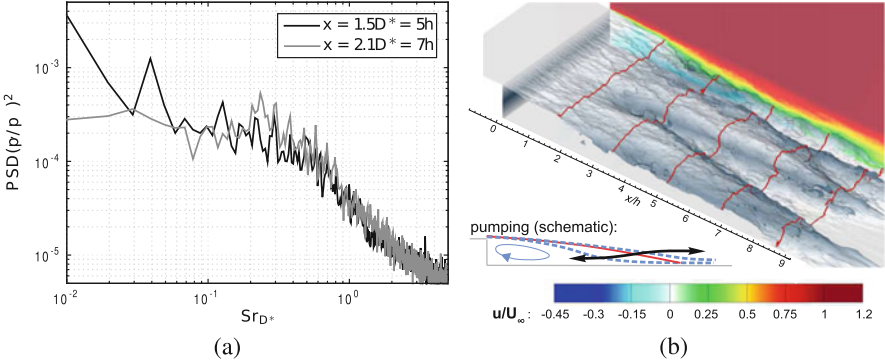


Fig. 2 (a) Power spectral density of wall pressure fluctuations p'/p_∞ . (b) Reconstruction of the first DMD mode describing a longitudinal pumping motion of the recirculation region at $Str_h \approx 0.01$ [27]

mean reattachment position $x = 2.1D^*$ reveals another dominant frequency at $Str_D^* \approx 0.23$. However, besides the detected frequencies no further information about the underlying coherent fluid motion, which would simplify the intricate wake flow physics down to a few degrees of freedom, is provided. Therefore, additional post-processing is required to extract the dominant spatio-temporal modes, which is done in the following by means of dynamic mode decomposition. The dynamic mode decomposition of the three-dimensional streamwise velocity field reveals two stable DMD modes at $Str_D^* = 0.037$ and $Str_D^* = 0.22$ closely matching the characteristic frequency ranges of the pressure fluctuations detected by the classical spectral analysis. To visualize the DMD modes it is superimposed with the mean mode and developed in time. The resulting flow field of the first DMD mode, which is shown in Fig. 1b, reveals that at the extracted frequency $Str_D^* \approx 0.037$ a coherent longitudinal pumping motion of the recirculation bubble takes place that is schematically sketched in the inlay of this figure. Thus, the mode captures a pronounced periodical low-frequency growth and subsequent collapse of the recirculation region in the streamwise direction between $4 \lesssim x_r/h \lesssim 9$, which leaves a clear trace in the wall pressure spectrum in Fig. 1a. Moreover, the obtained three-dimensional shape of the mode also explains the alternating formation of the elongated wedge-shaped coherent structures shown in Fig. 1b. Therefore, to indicate the pronounced three-dimensionality of the extracted longitudinal pumping mode given by the strong alternation in the spanwise direction the mode will be more precisely denoted as *cross-pumping*. A more detailed analysis of the performed investigations, i.e., a comparison between the presented planar BFS and an axisymmetric BFS configuration is given in [27, 28].

As outlined in the previous section, the wake of a space launcher is characterized by low frequency pressure oscillations arising due to large scale coherent motions which lead to undesired dynamic loads. For the development of future efficient lightweight space launchers it is essential to decrease these low frequency dynamic

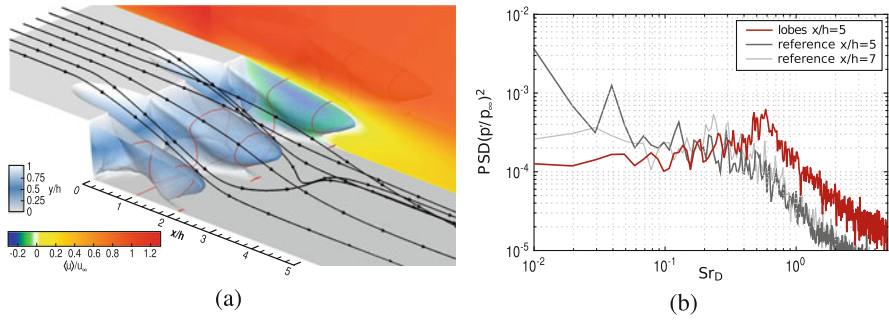


Fig. 3 (a) Flow topology of the time-averaged LES results. (b) Power spectral density of the wall pressure fluctuations p'/p_∞ at several streamwise positions for the lobe and reference configuration

loads. One promising possibility to manipulate the flow field and to reduce these loads is passive flow control. Therefore, a flow control device consisting of semi-circular lobes inserted at the trailing edge of the main body is investigated within the project. The aim of the applied loads is the generation of streamwise vortices which enhance the turbulent mixing directly behind the step and consequently, accelerates the reattachment process. The reduction of the reattachment length leads to an decreased lever arm and thus lower dynamic bending moments. Besides the reduction of the reattachment length, the lobes are to stabilize the large-scale coherent motion detected in the planar configuration described above.

To visualize the flow topology along the investigated configuration, Fig. 3a shows several characteristic streamlines and the streamwise velocity. The recirculation region is visualized by a iso-surface of the streamwise velocity $u/u_\infty = -0.01$ colored by the vertical distance from the nozzle surface. The intersection line of the velocity contour with the nozzle wall visualizes the reattachment of the flow and illustrates that averaged over time the shed shear layer impinges on the nozzle wall between $x_r/h \approx 1.3$ and $x_r/h \approx 2.3$ depending on the spanwise position. Recalling that the mean reattachment length of the planar BFS without flow control is $x/h = 7$, it is substantially reduced by more than 75% due to the lobes. In contrast to the reference case, the present configuration exhibits a pronounced three-dimensionality of the mean flow field characterized by the development of ellipsoidal reverse flow areas in the wake positioned in the spanwise direction between two adjacent lobes. A closer look at the streamlines shows that a part of the incoming boundary layer expands into the lobes, separates at the tail of the lobes, and flows straight to interact with the nozzle surface. At a streamwise position of about $x/h = 2$ this part of the flow possesses a strong spanwise velocity component such that pronounced streamwise vortices develop.

To evaluate the effect of the lobes on the pressure fluctuations, the power spectral densities (PSD) of the wall pressure signal at several streamwise positions are shown in Fig. 3b along with the previously shown spectra of the planar BFS without flow control. At the streamwise positions $x/h = 5$ and 7, where the lever arm of the

pressure fluctuations and thereby the resulting dynamic moments are largest, the spectra reveal that the low frequency pressure fluctuations and hence the undesired dynamic forces, which are responsible for the buffeting phenomenon, are reduced due to the semi-circular lobes. However, this reduction is achieved at the expense of increased high frequency pressure fluctuations at $St_D \geq 0.4$. Since these frequencies are not in the range of the eigenfrequencies of the thrust nozzle, the loads caused by these fluctuations do not impair the stability of the structure. In conclusion, the intended reduction of the reattachment length and the low frequency pressure fluctuations is achieved by means of the semi-circular lobes.

2.2 Supersonic Strut Supported Space Launcher Configuration

In this subproject, the turbulent wake of a supported wind tunnel model of a generic ARIANE 5-like space launcher with an underexpanded air nozzle jet is investigated at $Ma_\infty = 3$ and $Re_D = 1.3 \cdot 10^6$ to gain insight into the variation of intricate wake flow phenomena of space vehicles at higher stages of the flight trajectory with increasing Mach number. Since in the configuration with an air jet the ratio between the outer flow velocity and the nozzle exit velocity is significantly smaller compared to the one of a classical space launcher, the same configuration is investigated using a helium nozzle flow. Due to the smaller molar mass of the helium the nozzle exit velocity is strongly increased without changing the Mach number. In this way, the obtained velocity ratio is nearly similar with that of a classical space launcher. Due to the use of the helium nozzle flow, a multi-species version of the zonal flow solver is used in which the non-reactive gas mixtures is described by Fick's law. For further details the reader is referred to [13].

To illustrate the flow field topology around the investigated generic rocket model, the instantaneous Mach number in the symmetry plane and the wall pressure coefficient distribution on the wall are presented in Fig. 4. The topology shows a detached bow shock around the model's fairing which deflects the supersonic

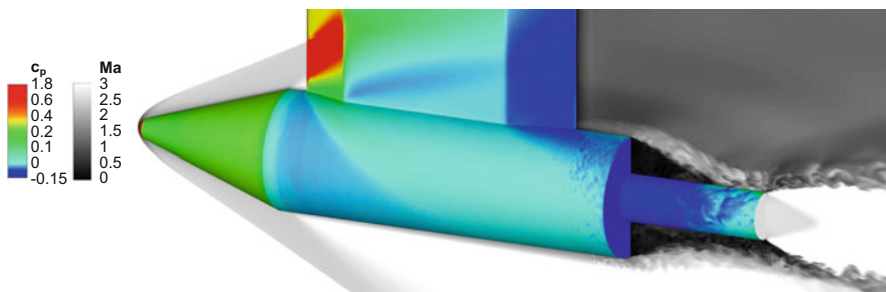


Fig. 4 Instantaneous Mach number (black and white) and wall pressure coefficient (color) distribution along the investigated generic space launcher configuration at $Ma_\infty = 3$ [29]

freestream parallel to the fairing’s walls and leads to a strong increase of the wall pressure coefficient. At the junction to the cylindrical part, the flow is redirected parallel to the freestream by an expansion fan causing the pressure to decrease again. Moving further downstream to the model’s tail, the turbulent supersonic boundary layer separates at the rocket model shoulder, forming a supersonic shear layer. As a result of the separation, the shear layer undergoes an expansion associated with a radial deflection towards the nozzle wall, leading to the formation of the low-pressure region and the subsonic recirculation zone. On the upper side of the configuration, a second shock and expansion wave system is formed around the double-wedge profiled strut which subsequently interacts with the shock and expansion waves emanating from the main body. A footprint of this interaction is the non-axisymmetric distribution of the pressure coefficient, shown in color in Fig. 4 on the launcher’s body. To validate the numerically computed wake topology, the density gradient obtained from the LES results is compared to the experimental Schlieren pictures in Fig. 5a and b for the air jet and helium jet configuration. Note that both the experimental and the numerical results are shown for the strut-averted side and the experimental pictures are mirrored for an easier comparison. The plume’s moderate afterexpansion leads to only a weak displacement effect, which results in the formation of a separation region with a triangular cross-section, having one large-scale vortex at the base and extending along the whole nozzle to its exit section. In the region close to the nozzle end the shear layer gradually realigns along the nozzle wall by weak recompression waves. The identical positions of the shock and expansion waves illustrate a good agreement between the experimental and numerical results with respect to the determined wake flow topologies. The obvious differences between the two cases is the intensity of the density gradient in the region of the nozzle exit and in the shear layer between the underexpanded jet plume and the outer flow. Due to the much larger density of the air in comparison to the helium, the density gradient is much smaller in the latter case. However, due to the supersonic outer flow the effect of the changed nozzle flow on the region further upstream is negligible. Thus, the position of the shear-layer, the expansion waves,

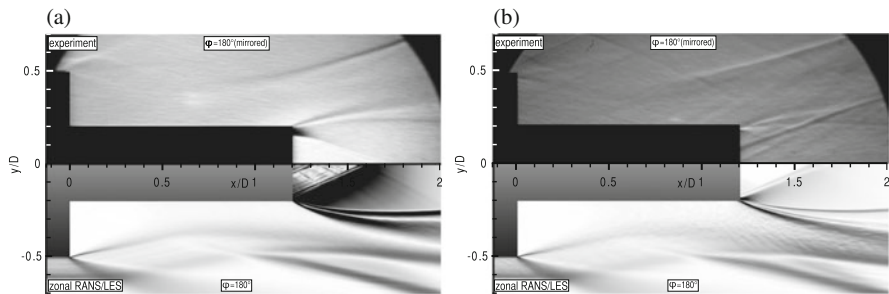


Fig. 5 Comparison of the experimentally and numerically obtained flow field topologies for the air flown nozzle (a) and the helium flown nozzle (b): Schlieren picture (top) and absolute density gradient of LES data (bottom) on the strut-averted side

and the shock, is nearly identical for the two different cases. A more extensive analysis of the supersonic strut supported space launcher configuration is given in [29]

2.3 Transonic Axisymmetric Space Launcher Configuration

After the investigation of the dynamic behavior of the wake flow of a generic planar configuration at the beginning of this chapter, the following part deals with the buffet flow of a space launchers. That is, a reduced-order analysis based on optimized DMD [19] is performed on the turbulent wake of a generic axisymmetric ARIANE 5-like configuration computed using the zonal RANS-LES method to investigate the buffet phenomenon of space launchers.

To visualize the flow topology the instantaneous spanwise vorticity distribution, time-averaged axial velocity profiles and streamlines are shown in Fig. 6a. The developed fully turbulent boundary layer separates at the axisymmetric shoulder and forms a turbulent free-shear layer. The shed shear layer rapidly evolves downstream of the separation due to the shear layer instability, causing the mixing layer and the turbulent structures to grow in size and intensity. This can be qualitatively identified in the development of the mean streamwise velocity profiles additionally shown in the lower part of Fig. 6a and in the plot of the Q-criterion iso-surface in Fig. 6b. Further downstream, the shear layer gradually approaches the nozzle and finally either impinges on its surface or passes over it, depending on the time instance and the azimuthal position, which will be discussed in the following.

The turbulent wakes of the investigated generic space launcher configurations are highly dynamic and are characterized by a manifold of spatio-temporal structures. For instance, the instantaneous streamline snapshots of the free-flight configuration

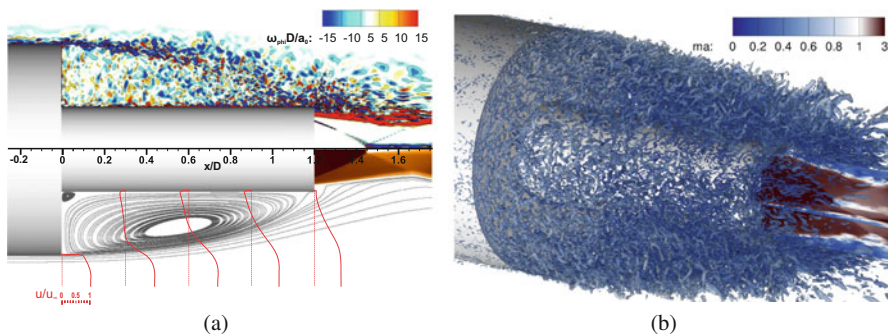


Fig. 6 Wake flow topology of the investigated free-flight configuration [30]: (a) instantaneous spanwise vorticity distribution (top); time-averaged axial velocity profiles and streamlines (bottom); (b) coherent structures in the wake visualized using Q criterion ($Q \cdot a_0^2 / D^2 = 300$) and color-coded by the Mach number

taken at the same azimuthal position $\varphi = 0$ at two time steps show in Fig. 7 that sometimes the shear layer reattaches onto the nozzle close to its center more than one step height upstream of the mean reattachment position or it does not reattach onto the nozzle but passing over it. Besides, the recirculation region incorporates a manifold of large-scale spanwise vortices of different sizes such that the time-averaged topology with only two toroidal vortices, illustrated in Fig. 6a, can be hardly identified. Furthermore, despite the axisymmetric geometry and zero angle of attack, the shed shear layer approaches the nozzle not axisymmetrically resulting in a pronounced asymmetry of the induced instantaneous azimuthal pressure distribution.

To provide insight into the temporal periodicity aspects of the wall pressure fluctuations, the power spectral density (PSD) distribution of the wall pressure signals is computed at several streamwise positions. Figure 8a shows the obtained spectra for the two previously defined characteristic positions, i.e., at the nozzle center ($x/D = 0.6$) and the mean reattachment position $x/D = 1.15$. At both

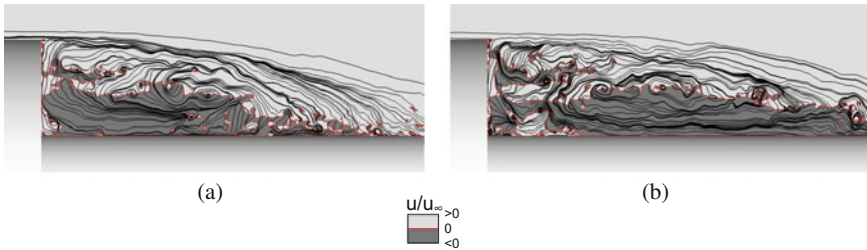


Fig. 7 Two-dimensional snapshots of the projected streamlines in the near wake at the azimuthal cut $\varphi = 0^\circ$ for two different time steps. The darker grey level in the field denotes backflow regions [30]

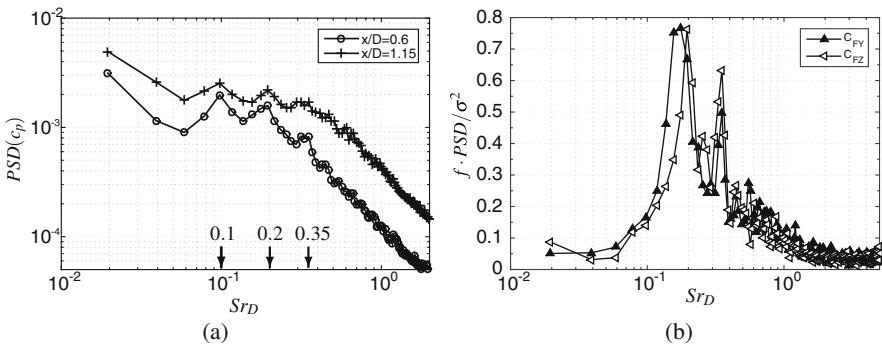


Fig. 8 Spatio-temporal spectral analysis of wall pressure fluctuations $c_{p'}$ on the nozzle [30]: (a) power spectral density (PSD); (b) premultiplied normalized power spectral density ($f \cdot PSD / \sigma^2$) of the side load components ($\sigma_{c_{p'y}} = 4.9 \cdot 10^{-3}$, $\sigma_{c_{p'z}} = 5.1 \cdot 10^{-3}$)

streamwise positions, two distinct peaks around $Sr_D \approx 0.1$ and $Sr_D \approx 0.2$ as well as a local broad-band plateau at $Sr_D \approx 0.35 \pm 0.05$ can be identified. Furthermore, an analysis of the spatial PSD function of the transposed space-time data matrix of the previously analyzed pressure values reveals the presence of a dominant antisymmetric $m_\varphi = 1$ mode that is followed by higher wave number modes with continuously descending amplitudes. The $m_\varphi = 1$ mode causes most critical side loads on the nozzle structure, while the higher wave number modes correspond to ovalization or buckling loads, i.e., modes $m_\varphi = 2$ or $m_\varphi \geq 3$. To get an insight into the buffet loads arising due to the previously mentioned pressure oscillations, the instantaneous load on the nozzle is computed by the surface integral of the instantaneous wall pressure field. The buffet loads feature a pronounced temporal periodicity. Figure 8b shows the frequency-premultiplied normalized PSD function for the two Cartesian components of the side force coefficient. The energetically most dominant frequency range at $Sr_D \approx 0.2$ is clearly seen. There is another pronounced but narrower and consequently, energetically less strong range around $Sr_D \approx 0.35$. Notice that these frequencies correlate with the respective values in the wall pressure fluctuations shown in Fig. 8a, while the low frequency peaks around $Sr_D \approx 0.1$ detected previously are hardly visible.

Optimized DMD is applied to the velocity field to extract phase-averaged modes for each of the three detected characteristic frequencies. Subsequently, a reduced-order analysis based on the extracted DMD modes is performed to scrutinize the underlying spatio-temporal coherent motion responsible for the buffet phenomenon. On the whole, three dynamic modes of interest, frequencies of which closely match the characteristic peaks in the wall pressure spectra and side loads, are identified in the DMD spectrum, i.e., $Sr_D(\lambda_1) \approx 0.1$, $Sr_D(\lambda_2) \approx 0.2$ and $Sr_D(\lambda_3) \approx 0.35$. The shape of these modes contains the information about the underlying phase-averaged coherent modulation of the flow field and is analyzed in the following.

The coherent phase-averaged fluid motion is obtained by superimposing the steady mean mode with the respective dynamic modes at the given frequency. The resulting reduced-order three-dimensional streamwise velocity fields are shown in Fig. 9 for the three frequencies of interest in ascending order, i.e., $Sr_D(\lambda_1) \approx 0.1$ (a), $Sr_D(\lambda_2) \approx 0.2$ (b), $Sr_D(\lambda_3) \approx 0.35$ (c). The first (top) row of the subplots shows the time instance t_0 , while the second (bottom) row illustrates the time instances $t_0 + 0.5T(\lambda_n)$, i.e., after one half of the respective period defined by $T(\lambda_n) = Sr_D(\lambda_n)^{-1}D/u_\infty$, to visualize the temporal evolution of the spatial modulation. Three types of coherent fluid motion are identified. The spatio-temporal modulation of the velocity field at $Sr_D \approx 0.1$ (Fig. 9a) indicates a longitudinal pumping motion of the recirculation region. At the second frequency of interest, $Sr_D \approx 0.2$ (Fig. 9b), a pronounced antisymmetric cross-flapping motion of the shear layer is clearly seen. At the third frequency, $Sr_D \approx 0.35$ (Fig. 9c), a quasi-swinging motion of the shear layer is extracted that occurs in phase with the previous flapping mode. In conclusion, the physical mechanism leading to the pressure oscillations and consequently the buffet loads can be traced back to the just detected motion of the recirculation region and shear layer. For a more detailed insight into the underlying mechanism of the buffet phenomenon see [25, 30]

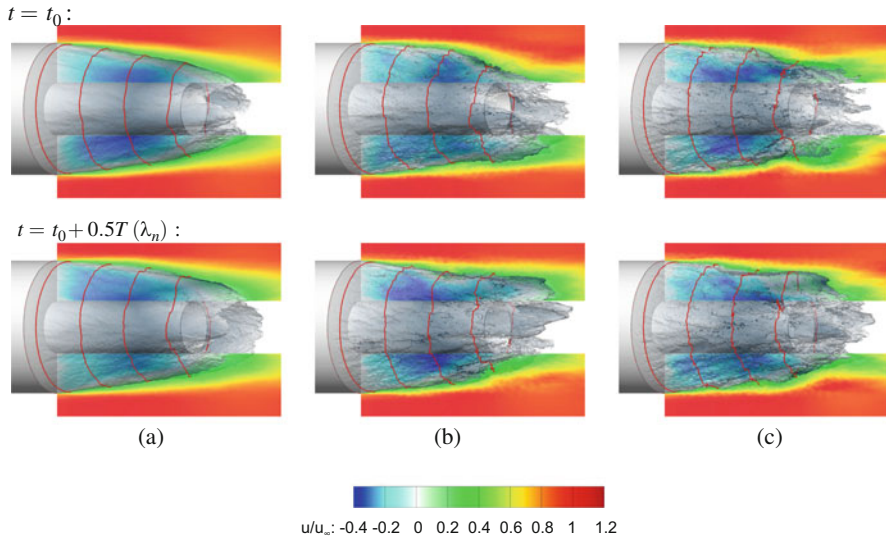


Fig. 9 Reduced-order modeled streamwise velocity field for the three characteristic frequencies [30]: (a) $Sr_D(\lambda_1) = 0.1$, (b) $Sr_D(\lambda_2) = 0.2$, (c) $Sr_D(\lambda_3) = 0.35$. Time instances at the beginning (top) and in the middle (bottom) of the respective period are shown

3 Computational Performance

The zonal computations as well as the subsequent DMD analyses have been performed on the CRAY XC40 (Hazel Hen) at the High-Performance Computer Center Stuttgart (HLRS, Stuttgart). The system consists of 7712 two socket nodes with 12 cores at 2.5 GHz. Each node is equipped with 128 GB of RAM, i.e., each core has 5.33 GB of memory available for the computations. In total a number of 185,088 cores with a peak performance of 7.42 Petaflops are available. The flow solver as well as the DMD postprocessor are optimized for the HLRS HPC system using hybrid parallelization based on MPI and OpenMP. Furthermore, parallel I/O procedure using HDF5 is employed.

To demonstrate the scalability of the used zonal RANS/LES flow solver, a strong scaling has been performed on the Hazel Hen. The scaling was performed on a cubic grid with 770^3 grid points. Six different core numbers were tested, i.e., 1008, 2016, 4032, 8064, 16,128 and 32,256. Each simulation runs for 1000 iteration steps and was repeated for multiple times to guarantee reproducibility. The overall speedup and the ideal speed up are given as a function of the number of cores in Fig. 10. The results prove the good scalability of the used code. For an exemplary analysis of the wake flow of an Ariane 5-like configuration [30], a zonal setup with approximately 500 Mio. grid points is used. The analyzed time-resolved data have been computed over a time interval of $409.6 t_{ref}$ after a transient phase of $100 t_{ref}$, with $t_{ref} = D/u_\infty$ being the reference time unit needed by a particle moving with the freestream

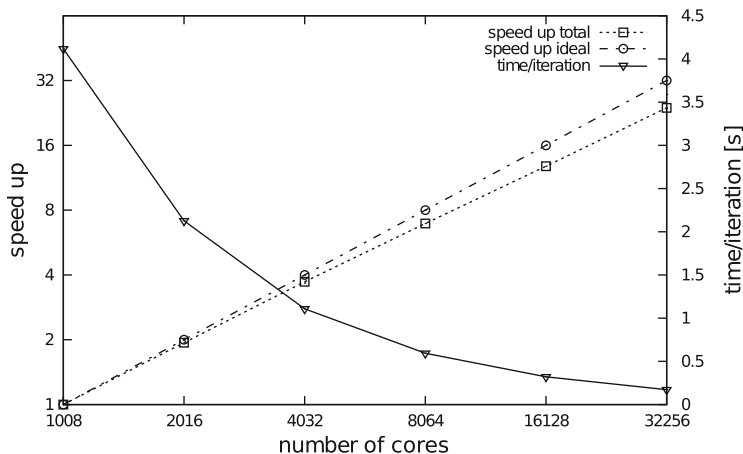


Fig. 10 Strong scaling experiment on Hazel Hen

velocity u_∞ to cover one reference length defined by the main body diameter. For this case, 14.6 Mio. core hours distributed over 9600 cores have been used in total.

4 Conclusion

Reduced-order analysis based on optimized dynamic mode decomposition has been performed on the turbulent wake of various generic space launcher geometries, including inter alia a planar backward-facing step configuration and an axisymmetric free flight launcher. The simulation has been performed using a zonal RANS/LES method. Both transonic and supersonic free stream conditions were considered. The results show a strong unsteady behavior of the recirculation region and shear layer leading to strong antisymmetric pressure loads on the nozzle extension. Using conventional statistical analysis, several characteristic frequencies were detected in the pressure signal of the different investigated configurations. To clarify the origin of the detected wake dynamics, the underlying spatio-temporal coherent modes were extracted using dynamic mode decomposition. Both, in the planar configuration and the axisymmetric free flight configuration a low frequency pumping motion of the recirculation region and a higher frequency flapping motion of the shear layer were identified which are responsible for the detected pressure fluctuations. Furthermore, a passive flow control device consisting of semi-circular lobes mounted on the base shoulder of the planar configuration was investigated. Due to this device, the reattachment length was reduced by up to 75%. In addition, the low frequency pressure oscillations which are mainly responsible for the buffet loads were slightly decreased by the lobes. However, this reduction was achieved at the expense of increased high frequency pressure fluctuations.

Acknowledgements Financial support has been provided by the German Research Foundation (Deutsche Forschungsgemeinschaft—DFG) in the framework of the Sonderforschungsbereich Transregio 40. The authors are grateful for the computing resources provided by the High Performance Computing Center Stuttgart (HLRS) and the Jülich Supercomputing Center (JSC) within a Large-Scale Project of the Gauss Center for Supercomputing (GCS).

References

1. I. Bolgar, S. Scharnowski, C.J. Kähler, Control of the reattachment length of a transonic 2d backward-facing step flow, in *International Conference on Jets, Wakes and Separated Flows* (2015)
2. P. Bradshaw, F. Wong, The reattachment and relaxation of a turbulent shear layer. *J. Fluid Mech.* **52**(1), 113–135 (1972)
3. S. Deck, P. Thorigny, Unsteadiness of an axisymmetric separating-reattaching flow: numerical investigation. *Phys. Fluids* **19**(065103), 65103 (2007)
4. D. Depres, P. Reijasse, J.P. Dussauge, Analysis of unsteadiness in afterbody transonic flows. *AIAA J.* **42**(12), 2541–2550 (2004)
5. D.M. Driver, H.L. Seegmiller, J.G. Marvin, Time-dependent behavior of a reattaching shear layer. *AIAA J.* **25**(7), 914–919 (1987)
6. J.K. Eaton, J.P. Johnston, A review of research on subsonic turbulent flow reattachment. *AIAA J.* **19**(9), 1093–1100 (1981)
7. E. Fares, W. Schröder, A general one-equation turbulence model for free shear and wall-bounded flows. *Flow Turbul. Combust.* **73**, 187–215 (2004). <http://doi.org/10.1007/s10494-005-8625-y>
8. R. Friedrich, M. Arnal, Analysing turbulent backward-facing step flow with the low-pass-filtered Navier-Stokes Equations. *J. Wind Eng. Ind. Aerodyn.* **35**, 101–128 (1990)
9. S.L. Gai, S.D. Sharma, Subsonic turbulent flow over a rearward facing segmented step. *Phys. Fluids* **27**, 544–546 (1984)
10. K. Isomoto, S. Honami, The effect of inlet turbulence intensity on the reattachment process over a backward-facing step. *J. Fluids Eng.* **111**, 87 (1989)
11. N. Jarrin, N. Benhamadouche, S. Laurence, D. Prosser, A synthetic-eddy-method for generating inflow conditions for large-eddy simulations. *Int. J. Heat Fluid Flow* **27**, 585–593 (2006)
12. H. Kaltenbach, G. Janke, Direct numerical simulation of flow separation behind a swept, rearward-facing step at $Re_\tau=3000$. *Phys. Fluids* **330**, 349–374 (2000)
13. M. Konopka, M. Meinke, W. Schröder, Large-eddy simulation of shock-cooling-film interaction at helium and hydrogen injection. *Phys. Fluids* **25**, 106101 (2013)
14. H. Le, P. Moin, J. Kim, Direct numerical simulation of turbulent flow over a backward-facing step. *J. Fluid Mech.* **330**, 349–374 (1997)
15. S. Marie, P. Druault, H. Lambare, F. Schrijer, Experimental analysis of the pressure-velocity correlations of external unsteady flow over rocket launchers. *Aerosp. Sci. Technol.* **30**, 83–93 (2013)
16. H. Park, W.P. Jeon, H. Choi, J.Y. Yoo, Mixing enhancement behind a backward-facing step using tabs. *Phys. Fluids* **19**, 105103 (2007)
17. B. Roidl, M. Meinke, W. Schröder, A reformulated synthetic turbulence generation method for a zonal RANS-LES method and its application to zero-pressure gradient boundary layers. *Int. J. Heat Fluid Flow* **44**, 28–40 (2013). <http://doi.org/10.1016/j.ijheatfluidflow.2013.03.017>
18. B. Roidl, M. Meinke, W. Schröder, Boundary layers affected by different pressure gradients investigated computationally by a zonal RANS-LES method. *Int. J. Heat Fluid Flow* **45**, 1–13 (2014)
19. P.J. Schmid, Dynamic mode decomposition of numerical and experimental data. *J. Fluid Mech.* **656**, 5–28 (2010)

20. F. Schrijer, A. Sciacchitano, F. Scarano, Experimental investigation of flow control devices for the reduction of transonic buffeting on rocket afterbodies, in *15th Symposium on Applications of Laser Techniques to Fluid Mechanics* (2010)
21. F. Schrijer, A. Sciacchitano, F. Scarano, Spatio-temporal and modal analysis of unsteady fluctuations in a high-subsonic base flow. *Phys. Fluids* **26**, 086101 (2014)
22. F.V. Silhan, J.M. Cabbage, Drag of conical and circular-arc boattail afterbodies at mach number of 0.6 to 1.3. *NACA RM L56K22* (1957)
23. A. Silveria Neto, D. Grand, O. Metais, M. Lesieur, A numerical investigation of the coherent vortices in turbulence behind a backward-facing step. *J. Fluid Mech.* **256**, 1–25 (1993)
24. R.L. Simpson, Turbulent boundary-layer separation. *Ann. Rev. Fluid Mech.* **21**, 205–2034 (1989)
25. V. Statnikov, Numerical analysis of space launcher wake flows, Ph.D. thesis, RWTH Aachen University, 2017
26. V. Statnikov, T. Sayadi, M. Meinke, P. Schmid, W. Schröder, Analysis of pressure perturbation sources on a generic space launcher after-body in supersonic flow using zonal RANS/LES and dynamic mode decomposition. *Phys. Fluids* **27**(016103), 1–22 (2015)
27. V. Statnikov, I. Bolgar, S. Scharnowski, M. Meinke, C. Kähler, W. Schröder, Analysis of characteristic wake flow modes on a generic transonic backward-facing step configuration. *Euro. J. Mech. Fluids* **59**, 124–134 (2016)
28. V. Statnikov, B. Roidl, M. Meinke, W. Schröder, Analysis of spatio-temporal wake modes of space launchers at transonic flow. *AIAA Paper 2016-1116* (2016)
29. V. Statnikov, S. Stephan, K. Pausch, M. Meinke, R. Radespiel, W. Schröder, Experimental and numerical investigations of the turbulent wake flow of a generic space launcher at $M_\infty = 3$ and $M_\infty = 6$. *CEAS Space J.* **8**(2), 101–116 (2016)
30. V. Statnikov, M. Meinke, W. Schröder, Reduced-order analysis of buffet flow of space launchers. *J. Fluid Mech.* **815**, 1–25 (2017)
31. I.A. Waitz, Y.J. Qiu, T.A. Manning, A.K.S. Fung, Enhanced mixing with streamwise vorticity. *Prog. Aerosp. Sci.* **33**, 323–351 (1997)